Traveling Wave based Wide Area Backup Protection for HVAC network interfacing MMC based HVDC system

Mahitosh Banafer, Soumya R. Mohanty, Tapan Prakash

***Abstract*—A robust & secured travelling wave (TW) based wide area backup protection scheme (WABPS) for mixed cable & overhead transmission line in HVAC grid interfacing MMC converter based HVDC grid is developed. A successive matrix pencil algorithm (SMPA) is used to estimate traveling wave arrival time (TWAT) at digital fault recorder (DFR) installed at AC buses. The estimated TWAT are next sent to the centralized graph theory based wide area real time fault localization tool for secured backup (zone-2 and zone-3) protection of the AC transmission system. The validation of proposed WABPS scheme is performed against different fault location, fault types, fault resistance as well as MMC converter control effects such as low voltage ride through (LVRT) capability.**

***Keywords*—Graph theory, hybrid AC/DC system, successive matrix pencil algorithm (SMPA), traveling wave (TW), wide area backup protection scheme (WABPS).**

I. Introduction

THE AC transmission lines and cables are generally exposed to disturbances, which can threaten the power system security unless protected by a robust transmission line protection scheme. The conventional distance protection scheme may maloperate due to under reach, over reach, load encroachment and power swing which may lead to power system outages such as USA 2003 and India 2012 blackout [1]. The modern day power system is evolving to a hybrid AC/DC grid with integration of voltage source converter (VSC) based high voltage DC (HVDC) transmission system [2].

A. Motivation and Incitement

The grid fault characteristics of the hybrid AC/DC transmission system will be different from traditional HVAC grid. The integration of HVDC transmission line leads to low short circuit ratio (SCR) [3], which will impact the behaviour of distance relaying scheme due to limited fault current from modular multilevel converter (MMC) [4], [5]. Moreover, low inertia in a hybrid AC/DC system may lead to more frequency instability, incorrect memory polarization and remote infeed issues which can cause distance relay maloperation [6].

As per the grid code requirement, during short circuit fault near point of common coupling (PCC), the reactive power control of MMC converter is activated to boost the PCC bus voltage which is known as low voltage ride through (LVRT) control. The impact of MMC's LVRT control on distance protection scheme will be very much significant [7] and there is a need to develop a robust and secure protection scheme for hybrid AC/DC system.

B. Related Works

The backup zone of the distance protection schemes are generally more prone to system stressed conditions such as load encroachment, power swing and voltage instability, and which is further aggravated by the MMC converter interfaced HVDC link. To solve this issue, a two criteria approach is used to discriminate system stressed conditions from symmetrical fault for secured backup protection element [8]. But it did not considered the effects of MMC converter based HVDC link control dynamics on the backup protection zone. Therefore, an accurate impedance measurement based backup protection scheme is formulated to avoid miss-coordinated zone identification in distance relaying scheme [7]. But its study is only limited to reactive power control of VSC converter and lacks detailed discussions on its effect on backup protection scheme. Another fast communication assisted distance protection for HVAC line emanating from MMC-HVDC station is proposed by [9]. Its protection criteria is based on polarity direction factor & comparison of measured and projected reference impedance at the relay location. Its main limitations are communication dependence, delayed response for primary protection of some high resistive symmetrical fault.

In summary, the protection of HVAC transmission line interfacing with MMC based HVDC link can be broadly classified into adaptive protection-based [10], robust control-based [11], differential protection-based [12], integrated AC/DC protection [13], wide area phasor measurement unit (PMU)-based [14], traveling wave (TW)-based [15], and machine learning based protection scheme [14]. Out of these, the PMU-based wide area protection is the most widely suggested backup protection scheme for HVAC transmission line. For secured relaying operation, the conventional distance relay is supervised using wide area deep neural network (DNN) based wide area backup protection scheme (WABPS) to prevent relay maloperation under system stressed conditions [14]. Although it is resilient to high impedance and noise contaminated signal, but it also has shortcoming such as limited scalability, system topology dependence, intensive training and detailed system modelling requirement. Another secured adaptive protection scheme is formulated using phase angle of the faulted current loop to determine pure fault impedance for correct relay zone

Mahitosh Banafer and Soumta R. Mohnaty is with the Department of Electrical Engineering, Indian Institute of Technology (BHU) Varanasi, India (e-mail of corresponding author: mahitosh.banafer.rs.eee18@iitbhu.ac.in, tapan.prakash@vit.ac.in). Tapan Praksh is with the School of Electrical Engineering, VIT university, Vellore, India.

Paper submitted to the International Conference on Power Systems Transients (IPST 2025) in Guadalajara, Mexico, June 8-12, 2025.

identification [10]. But it might not work satisfactorily for noise contaminated voltage signal due to poor performance of conventional signal processing technique. To overcome this issue, a robust control based MMC converter unit is suggested for hybrid AC/DC system to avoid conventional distance relay malopeartion [11]. But it is only validated for low fault resistance and it might not work satisfactorily for high fault impedance.

The TW principle is generally used for fault localization and researchers have also suggested TW based primary protection for HVAC transmission line recently [15]. Apart from the TW-based primary protection, very few researchers have also explored the TW-based wide area protection and fault localization schemes for HVAC transmission line [16]. It have mostly explored the suitability of IEC-61850 communication protocol for TW-based WABPS using high sampling frequency measurements (up to 500 kHz), but it have not studied its suitability for backup protection of MMC converter interfaced HVAC grid under low sampling frequency measurement (50 kHz). Moreover, the offshore wind farm integrated HVAC system requires overhead transmission line and submarine cables, but very few protection schemes are developed for hybrid overhead transmission line and cable system. The TW based fault localization scheme for hybrid transmission line is derived using wavelet transform technique in [17], but protection aspects are not explored.

C. Contribution

The main contributions of the paper are -

1) A novel secured TW based wide area backup protection scheme for mixed cable & overhead transmission line (OHTL) of AC grid interfacing MMC based HVDC link is designed, which is robust against MMC control schemes such as LVRT.
2) The successive matrix pencil algorithm (SMPA) and linear regression tool is used to extract TWAT information in the digital fault recorder (DFR) installed at the local AC terminal bus using low sampling frequency measurement (50 kHz) as opposed to other traveling wave arrival time (TWAT) based scheme discussed in literature.

II. Proposed TW based WABPS for HVAC grid interfacing HVDC link

A. Low sampling frequency TW arrival time estimation

1) Pre-processing of relay input signal: To eliminate mutual coupling effect between measured three phase voltage signal, a modal transformation (Karenbauer transformation) equation is used prior to TW arrival time (TWAT) estimation as shown in (1) -

$$\begin{bmatrix} u_\alpha \\ u_\beta \\ u_0 \end{bmatrix} = \frac{1}{3} \begin{bmatrix} 1 & -1 & 0 \\ 1 & 0 & -1 \\ 1 & 1 & 1 \end{bmatrix} \begin{bmatrix} u_a \\ u_b \\ u_c \end{bmatrix} \tag{1}$$

Here, u_α (relaying signal input), u_β are aerial mode and u_0 is the ground mode voltage signal respectively, whereas u_a, u_b and u_c are the three phase AC voltage measured at the DFRs located at transmission line or cable terminal end.

2) Successive matrix Pencil algorithm (SMPA) based TWAT estimation: In next step, it is quite prudent to extract TWAT information from u_α using signal processing techniques. A band limited signal in a time period T, such as u_α, can be expressed as weighed summation of damped sinusoids or cosinusoids as shown below -

$$u_\alpha(t) = \sum_{m=1}^{M} A_m e^{-\alpha_m t} \sin(\omega_m t + \phi_m) \tag{2}$$

Here M is the number of sinusoids along with residue $A_m \angle \phi_m$. Whereas α_m (s^{-1}) and ω_m are the real part (damping factor) and imaginary part (angular frequency) of the m^{th} complex frequency $(\alpha_m \pm j\omega_m)$ component. Short time discrete Fourier transform (STDFT) is generally used for residue and frequency estimation, whereas subspace based technique such as matrix pencil algorithm (MPA) [18] is used for complex frequency and residue estimation for (2).

Since, MPA or any other subspace based method uses dual degree of freedom (damping factors & sinusoids) and DFT uses only sinusoids for signal reconstruction [18]. As evident from Fig. 1(a), the matrix pencil algorithm (MPA) can reconstruct the pulse signal (TW) more effectively than discrete Fourier Transform (DFT) technique. The MPA method is applied to the TW samples inside a fixed size window extracting time-indexed complex frequency components, which slide along the time axis and it is called successive MPA (SMPA) technique as shown in Fig. 1(b). When the pulse signal (TW) enters the moving window, then the extracted damping factor (α) is positive, zero and negative for position of TW as right, center and left in the moving window respectively as shown in Fig. 1(c).

This principle can be used to extract arrival time (AT) of the TW (pulse), positioned as shown in Fig. 1(a) as -

$$\alpha_m = 0, \forall m \rightarrow AT = t_0 + T_w/2 \tag{3}$$

Where α_m, AT, t_0 and T_w are the extracted damping factor, arrival time of the TW (pulse), position and width of the moving window respectively as described in Fig. 1(b).

For damping factor (α_m) extraction via SMPA method, a Hankel matrix $Y_{(N-L)X(L+1)}$ is formed using samples of u_α inside a N sample sized window, which is -

$$Y = \begin{pmatrix} u_\alpha(1) & u_\alpha(2) \cdots\cdots\cdots & u_\alpha(L+1) \\ u_\alpha(2) & u_\alpha(3) \cdots\cdots\cdots & u_\alpha(L+2) \\ \vdots & \vdots & \vdots \\ u_\alpha(N-L) & u_\alpha(N-L+1) \cdots & u_\alpha(N) \end{pmatrix} \tag{4}$$

Where $u_\alpha(.)$ & N represents aerial mode voltage signal sample value and number of signal samples inside the moving window respectively. The pencil parameter value (L) is advised to kept in between $N/2$ and $N/3$ for efficient noise filtration [17], [19]. Conventionally, singular value decomposition (SVD) is applied to matrix Y -

$$Y = USV^H \tag{5}$$

$$\sigma_s = 10^{-p} \sigma_{s\max} \tag{6}$$

Here, U, V are the unitary matrices, whose elements are

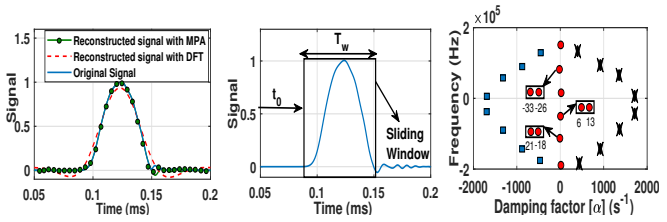

(a) (b) (c)

Fig. 1. (a) Reconstructed pulse signal (TW) by SMPA and short time discrete Fourier Transform (STDFT) with the same number of terms of sinusoids. (b) Pulse-shape signal and sliding window. (c) Complex frequencies extracted by applying SMPA to the pulse shown in (b).

eigenvectors of YY^H and Y^HY respectively. The S is a diagonal matrix which elements are the eigenvalue of Y and $(.)^H$ represents the complex conjugate transpose operation on the matrix. In (5), the σ_s and $\sigma_{s\max}$ are the singular value elements and the largest singular value elements of matrix S. The parameter p is the filtering parameter which is used to separate signal and noise subspace matrices for further analysis.

Further, matrix S is reduced to S' by saving its content corresponding the dominant singular value. In similar fashion, a new matrix V' is also formed from the matrix S [18].

$$\begin{aligned} Y_1 &= US'V_1^{'H} \\ Y_2 &= US'V_2^{'H} \end{aligned} \tag{7}$$

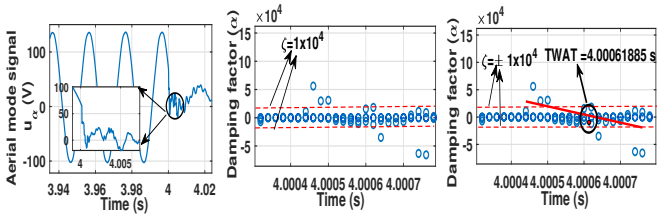

(a) (b) (c)

Fig. 2. (a) Aerial mode voltage signal (u_α). (b) Damping factor-time diagram obtained by applying SMPA algorithm. (c) The fitted line to the dispersed damping factors (using linear regression), and its ZCP (TWAT) estimation.

After that, the eigenvalue of $Y_1{}^+Y_2$ ($(.)^+$ represent pseudo inverse operation) is used to find the complex frequencies of the windowed signal, as shown below -

$$\lambda_m = e^{(-\alpha_m \pm j\omega_m)T_s}, \forall m = 1, 2, 3.....n \tag{8}$$

Here, λ_m and T_s is the eigenvalue of $Y_1{}^+Y_2$ and sampling time period respectively. In the next step, the time indexed complex frequency is extracted using λ_m as shown below -

$$\alpha_m(t) \mp j\omega_m(t) = -\ln(\lambda_m)/T_s, \forall m = 1, 2, 3...n \tag{9}$$

The SMPA is used to extract time indexed damping factor (α_m) from the sliding window as shown in Fig. 2(a) and (b). A threshold ($\zeta = \pm 1 \times 10^4$) is used for applying the linear regression method to the damping factor estimated by SMPA in order to estimate the TWAT, as shown in Fig. 2(b) and (c). The threshold (ζ) is determined empirically for the test system by simulating the highest fault resistance at the farthest fault location under maximum noise conditions. If the damping factor is greater than ζ, the linear regression method is applied to estimate the TWAT or the zero-crossing point (ZCP) of α_m, as shown in Fig. 2(b) and according to (3). The linear regression tool is used for accurate estimation of the ZCP of α_m as shown in Fig. 2(c).

$$\alpha_d(t) = a_0 + a_1 t + \varepsilon_d(t), \forall t \in (t_1, t_2), \forall m \tag{10}$$

Here t_1 and t_2 are the start and end timestamp of the dispersed time indexed damping factor α_d as shown in Fig. 2(c). a_1 (slope) and a_0 (constant) are the linear regression coefficient, whereas $\varepsilon_d(t)$ is the linear regression error term. The matrix form of (10) can be re-written as -

$$\alpha_d = t_d a + \varepsilon \tag{11}$$

Here $\alpha_d = [\alpha_m(t_1), ..., \alpha_m(t_2)]^T$ is the vector of time indexed dispersed damping factor, $a = [a_0, a_1]^T$ is the matrix of linear regression coefficient, $\varepsilon = [\varepsilon_d(t_1), ..., \varepsilon_d(t_2)]^T$ is the error vector and $t_d = \begin{bmatrix} 1.....1 \\ t_1.....t_2 \end{bmatrix}^T$ is the time vector. The regression coefficient of (11) can be calculated by solving -

$$\hat{a} = (t_d^T t_d)^{-1} t_d^T \alpha_d \tag{12}$$

Where $\hat{a} = [\hat{a}_0, \hat{a}_1]^T$ is the estimated linear regression coefficient from (12) and $(.)^T$ is the matrix transposition operation. The ZCP (TWAT) of α_d is given as -

$$TWAT = -\frac{\hat{a}_0}{\hat{a}_1} \tag{13}$$

Moreover, the fault location error (FLE) is -

$$FLE = \frac{|AFL - CFL|}{l} * 100 \tag{14}$$

Where, AFL and CFL are the actual and calculated fault location of the AC fault in the HVAC grid and L is the length of AC transmission line or cable.

B. TWAT based WABPS Using Graph Theory

1) Graph theory Representation of VSC Interfaced HVAC Grid: Any HVAC part of the hybrid AC/DC system can be represented by a un-directed weighted graph $g = (n, b, w)$, where $n = \{n_1, n_2, n_3, ...\}$, $w = \{w_1, w_2, w_3, ...\}$ and $b = \{b_1, b_2, b_3, ...\}$ are the set of nodes, weights and branches respectively. In a weighted graph g, $P^{min}_{n_1,n_2}$ is used to represent the shortest path between two nodes n_1 and n_2. Moreover, the distance between nodes n_1 and n_2 can be defined as sum of weights of branches involved in $P^{min}_{n_1,n_2}$ [20], which is denoted as D_{n_1,n_2}. The weighted graph g is systematically sectionalize

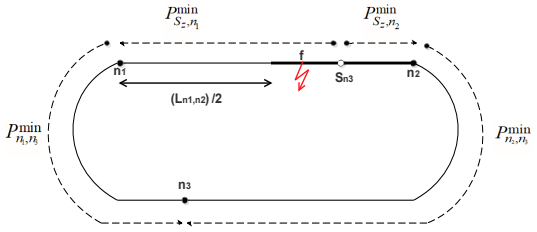

Fig. 3. Locus of symmetric point S_{n3} in graph G.

for WABPS using two lemmas [20] which are -

Lemma I : If a point f lies on the shortest path between two arbitrary nodes n_1 and n_2 on the graph g, then this path

can be represented as the union of the shortest path between node n_1 and f, and the one between f and n_2.

Lemma II : Assuming a branch between nodes n_1 and n_2, i.e..; $(n_1, n_2) \in b$. For any shortest path between nodes n_2 and n_3 passes through node n_1, then for any random point f on the branch (n_1, n_2), the node n_1 must lie on the shortest path between f and n_3.

TW will always travel the shortest path from the fault point to the DFR location and its velocity in each branch (transmission line/cable), (n_1, n_2), is denoted by v_{n_1,n_2}. The weight of each branch (n_1, n_2) of graph g is multiplied by $v_0/v_{n_1,n_2}$ for normalization, where v_0 is the base TW velocity. Suppose a line with different segments connects two nodes n_1 and n_2, and a detector is located at terminal n_3 as shown in Fig. 3. The shortest path and distance from the fault point f to transient detector location n_3 is calculated as -

$$\begin{aligned} P^{min}_{f,n_3} &= min(P^{min}_{f,n_1} \cup P^{min}_{n_1,n_3}, P^{min}_{f,n_2} \cup P^{min}_{n_2,n_3}) \\ D_{f,n_3} &= min(D_{f,n_1} \cup D_{n_1,n_3}, D_{f,n_2} \cup D_{n_2,n_3}) \end{aligned} \tag{15}$$

The conditions under which both the values in (15) are equal and S_{n_3} be the symmetric point between P_{n_1,n_2}, which hold equality constraint condition. By equating this two values -

$$D_{S_{n_3},n_1} = \frac{D_{n_2,n_3} - D_{n_1,n_3} + D_{n_2,n_1}}{2} \tag{16}$$

The symmetric point S_{n_3}, whose shortest distances from node n_3 exist in two possible directions, one traverses through node n_1 and another through n_2, which can be determined from (16). As per *Lemma II*, the shortest path from each arbitrary point f on segment (S_{n_3}, n_1) to the node n_3 would surely contains node n_1. Similarly, the shortest path between any arbitrary point f on line segment (S_{n_3}, n_2) to node n_3 would pass through the node n_2.

let's assume I to be a set having indices of all nodes equipped with DFR. Suppose for branch (n_1, n_2), the symmetric point S_{n_3} is found for detector at node $n_3 \in I$, then the branch (n_1, n_2) will be sectionalized into at most $|I| + 1$ segments. Here, $|I|$ represents the number of elements in the sets, i.e.; also known as cardinality of I. Therefore, for any fault point f on the line segment (n_x, n_y), it is pre-decided whether the shortest path will traverse the node n_1 or n_2, and it is to be noted that this property is independent on the location of f on the (n_x, n_y) segment. The wide area backup protection strategy (WABPS) involves mainly two stages as -

2) Fault Equations for Different Segments of VSC Converter Interfaced HVAC System: Let (n_x, n_y) be the line segment on the branch (n_1, n_2) of graph g, and $I^{(n_x,n_y)}_{n_1}$ & $I^{(n_x,n_y)}_{n_2}$ are the sets of all detectors where the TW surge emanating from f on segment (n_x, n_y) traverses through node n_1 and n_2 in their path respectively. It can also be mentioned that -

$$I^{(n_x,n_y)}_{n_1} \cup I^{(n_x,n_y)}_{n_2} = I \tag{17}$$

The following two group of TWAT equations can be formulated -

$$\begin{aligned} t^{AT}_i &= t_0 + \tfrac{D_{f,n_1}}{v_0} + \tfrac{D_{n_1,i}}{v_0}, \forall i \in I^{(n_x,n_y)}_{n_1} \\ t^{AT}_i &= t_0 + \tfrac{D_{f,n_2}}{v_0} + \tfrac{D_{n_2,i}}{v_0}, \forall i \in I^{(n_x,n_y)}_{n_2} \end{aligned} \tag{18}$$

Where, t^{AT}_i is the first TWAT at detector location i. It can be further deduced that $L_{n_1,n_2} = D_{f,n_1} + D_{f,n_2}$, as the fault point f lies on the line/branch (n_1, n_2). There are also some topology dependent parameters, such as $T_{n_1,n_2} = L_{n_1,n_2}/v_0$, $T_{n_2,i} = D_{n_2,i}/v_0$ and $T_{n_1,i} = D_{n_1,i}/v_0$. And the unknown term $D_{n_1,f}/v_0$ in (18) is expressed as t_{f,n_1} and the rewritten set of equations are -

$$\begin{aligned} t^{AT}_i - T_{n_1,i} &= t_0 + t_{f,n_1}, \forall i \in I^{(n_x,n_y)}_{n_1} \\ t^{AT}_i - T_{n_2,i} - T_{n_1,n_2} &= t_0 - t_{f,n_1}, \forall i \in I^{(n_x,n_y)}_{n_2} \end{aligned} \tag{19}$$

To solve (19), the shortest path and the distance between all node pairs (all $D'_{n_1,n_2}s$) need to found first, which can be achieved using the efficient algorithm proposed in [20]. The (19) can be further simplified in the matrix form as -

$$N = \begin{bmatrix} H^{(n_x,n_y)}_{n_1} \\ H^{(n_x,n_y)}_{n_2} \end{bmatrix} \times \begin{bmatrix} t_0 \\ t_{f,n_1} \end{bmatrix} \tag{20}$$

Where N is a measurement matrix of size $(|I|^{(n_x,n_y)}_{n_1} + |I|^{(n_x,n_y)}_{n_2})X1$ and the $H^{(n_x,n_y)}_{n_1}$ & $H^{(n_x,n_y)}_{n_2}$ are generally represented as-

$$H^{(n_x,n_y)}_n = \begin{bmatrix} 1 & 1 \\ \vdots & \vdots \\ 1 & 1 \end{bmatrix}_{\left|I^{(n_x,n_y)}_n\right| \times 2}$$

(20) is the set of two linear equations with two unknown variables (inception time and real time fault distance), which can be solved using least square technique for the fault f on line segment (n_x, n_y). Finally, the real time fault distance on transmission line (branch) (n_1, n_2) is calculated as $v_{n_1,n_2} \cdot t_{f,n_1}$, where v_{n_1,n_2} is the TW velocity in branch (n_1, n_2)

3) Fault Segment Identification for WABPS: A wide area real time fault distance is calculated by solving (20) for a fault on the line segment on sectionalized graph g. But, the faulted segment is not known prior to solving (20). Therefore, the faulted line segment is identified by subtracting all possible equations pair in (19) as shown below -

$$\begin{aligned} t^{AT}_i - t^{AT}_j &= T_{n_1,i} - T_{n_1,j}, \forall i,j \in I^{(n_x,n_y)}_{n_1} \\ t^{AT}_i - t^{AT}_j &= T_{n_2,i} - T_{n_2,j}, \forall i,j \in I^{(n_x,n_y)}_{n_2} \end{aligned} \tag{21}$$

It can be pointed out that the AT difference between specified detector pair i & j is not dependent on line segment (n_x, n_y). Therefore, for all line segment (n_x, n_y) located on branch (n_1, n_2), the following equations is constituted for TWAT at different detector location -

$$\begin{aligned} &\sum_{\forall i,j \in I^{(n_x,n_y)}_{n_1}} |(t^{AT}_i - t^{AT}_j) - (T_{n_1,i} - T_{n_1,j})| \\ &+ \sum_{\forall i,j \in I^{(n_x,n_y)}_{n_2}} |(t^{AT}_i - t^{AT}_j) - (T_{n_2,i} - T_{n_2,j})| \end{aligned} \tag{22}$$

As per (21), if fault is on line segment (n_x, n_y), then (22) would be equal to zero, maybe small positive number due to rounding off error and measurement errors. hence, the faulted line segment is identified, which is prerequisite for identifying real time fault distance in WABPS.

C. Proposed TW based WABPS

The proposed protection scheme has two stages -

Offline Stage:

1) The graph topology of the HVAC part of the hybrid AC/DC grid is derived, which is generally fixed.
2) Considering the location of DFRs, all branches of the derived graph topology are sectionalized using (16). A set B^{new} is formed containing all segments whose terminal ends are either node or symmetrical nodes on the branch.
3) For all segment, i.e.; $\forall(n_x, n_y) \in B^{new}$, with respect to the branch under study say (n_1, n_2), the set I_{n1} and I_{n2} are obtained as explained in previous section.

Online Stage (WABPS):

1) The TWATs are estimated at different DFR location across HVAC side of the hybrid AC/DC system using proposed technique low sampling frequency (50 kHz) measurements.
2) For all offline identified segments, i.e.; $\forall(n_x, n_y) \in B^{new}$, (22) is calculated and the lowest among all would be considered as the faulted segment.
3) In the next step, the system of equations (19) for the identified line segment, in previous step, is solved to estimate real time fault location, and a backup trip signal is sent for secured backup protection.

In summary, the installed DFRs at different bus location records the precise TWAT using SMPA algorithm. The estimated TWAT is retrieved from multiple wide-area sensors (DFRs) via IEC-61850 compliant communication channel and real time fault location is calculated using a graph theory-based method. By analyzing the time differences and the known network topology, the fault location can be quickly and accurately identified on real time basis. The real-time fault location using TWATs can support distance-based backup protection in HVAC transmission lines, thus improving the speed and reliability of backup protection schemes.

III. Test Hybrid AC/DC System

To evaluate the performance of proposed TW based WABPS, a test hybrid AC/DC transmission system is modeled as shown in Fig. 4(a). The detailed description of hybrid AC/DC grid parameters are tabulated in Table I.

TABLE I
MMC Converters and AC/DC Grid Parameters

Converter and grid parameters	Converter 1	Converter 2
Rated power (MVA)	1500	1500
AC grid voltage (kV)	400	400
DC grid voltage (kV)	± 320	± 320
Control mode	V_{AC} and V_{DC}	P and Q
AC converter ratio (Grid/VSC)	400/175	400/175
Frequency (Hz)	50	50
Arm capacitance (μF)	33.5	33.5
Arm reactor (mH)	50	50
Arm resistance (Ω)	0.385	0.385
Bus filter reactor (mH)	15	15

The DFRs are installed at all AC buses as shown in Fig. 4(a), which is equipped with proposed TWAT estimation tool requiring 50 kHz sampling frequency. For fault F_1 and F_2 in the test hybrid AC/DC grid shown in Fig. 4(a), the time synchronized TWAT information extracted at the installed DFRs are transferred to the graph theory based centralized WABPC via dedicated communication channel conforming to IEC-61850 GOOSE message protocol as shown in Fig. 4(b). As clear from Fig. 4(b), the symmetrical nodes for node "B", "C" and "D" are S_{zb}, S_{zc} and S_{zd} respectively. The location of S_{zb}, S_{zc} and S_{zd} from AC bus B are 59.5 km, 39.5 km and 15.2 km respectively, which is calculated using (16). The symmetrical nodes for node B and D lies in L_{23}, instead of L_{26} and L_{36}, due to traveling wave velocity parity between short length cable and OHTL. Therefore, symmetrical nodes S_{zb} and S_{zd} are redundant and only S_{zc} will be considered for sectionalizing line L_{34} in two sections $L_{B,S_{zc}}$ and $L_{S_{zc},D}$.

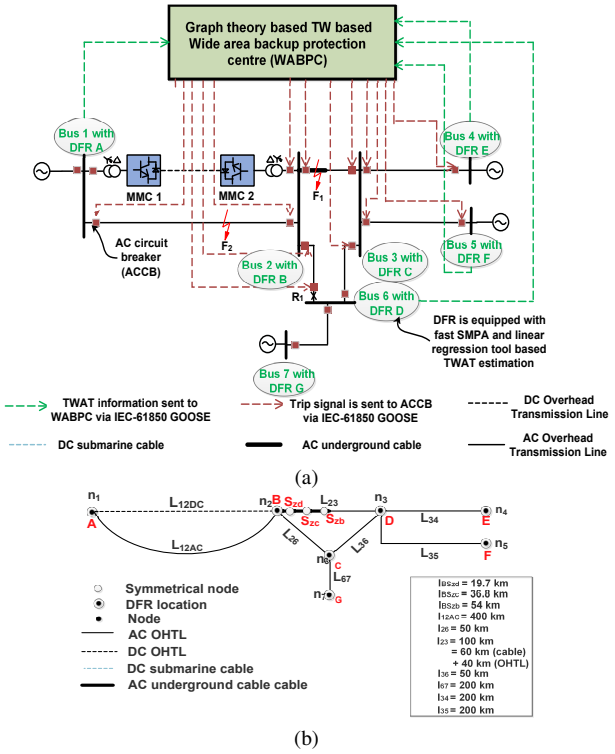

Fig. 4. (a) Schematics of proposed WABPS for test hybrid AC/DC grid interfacing offshore wind farm. (b) Associated sectionalized graph representation.

IV. Simulation Results and Discussion

The hybrid AC/DC transmission system shown in Fig. 4 is modeled in PSCAD/EMTDC software. The half bridge MMC converter model is developed using continuous equivalent MMC model with blocking/de-blocking and LVRT capability. The overhead transmission line (OHTL) and cable are modeled using frequency dependent (phase) models. The TW velocity for the cable & OHTL is found to be 121.30 km/ms and 255.219 km/ms respectively. The simulation time step is selected as 20 μs corresponding to 50 kHz sampling frequency measurement and signal-to-noise- ratio is considered to be 50 dB for all simulation cases analyzed and discussed in this section. The matrix Y of SMPA technique (used for proposed WABPS) has dimensions of 5X6, based on the chosen values of $N = 10$ and $L = 10$, with a filtering parameter P set to 3. Moreover, the predetermined threshold (ζ) for the test system is empirically determined by simulating a 100 Ω (highest) fault

resistance in OHTL/cable at farthest fault location under 50 dB SNR (worst) noise contaminated signal.

A. Impact of fault location

To study the impact of fault location on the proposed TW based WABPS, a three phase (LLL) fault is simulated at 0.7s in F_1 with varying fault distance in AC cable and OHTL between AC bus 2 and 3 as shown in Fig. 4(a). At first, the fault location is set at 48 km from AC bus 2 in cable part of the mixed cable/OHTL between AC bus 2 and 3 in test hybrid AC/DC system. The SMPA based algorithm employed inside the DFRs installed at the AC buses are shown in Fig. 5.

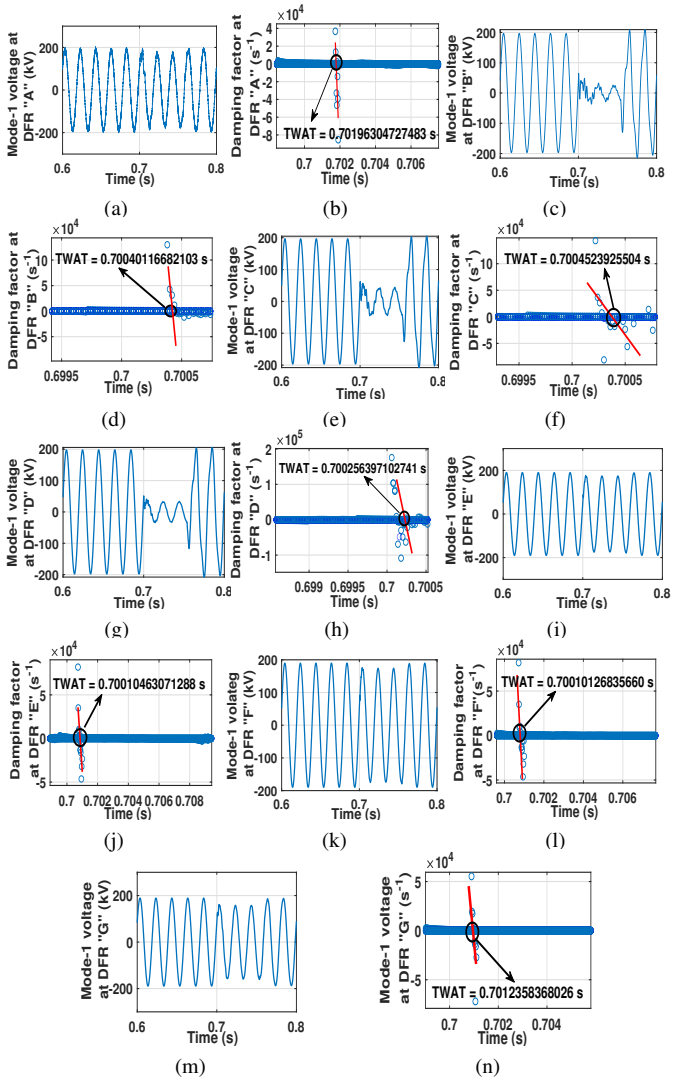

Fig. 5. SMPA performance (a) u_α at DFR "A", (b) TWAT at DFR "A", (c) u_α at DFR "B", (d) TWAT at DFR "B", (e) u_α at DFR "C", (f) TWAT at DFR "C", (g) u_α at DFR "D", (h) TWAT at DFR "D", (i) u_α at DFR "E", (j) TWAT at DFR "E", (k) u_α at DFR "F", (l) TWAT at DFR "F", (m) u_α at DFR "G", (n) TWAT at DFR "G".

The extracted TWATs at all 7 DFRs for fault induced TW are sent to WABPC, where graph theory algorithms are used to identify the fault segment and real time fault localization. (22) is used to identify (coarse estimation) the faulted segment in the HAVC network, whereas (20) is used to estimate the real time fault location. If the CFL falls in the protected zone for zone-2 and zone-3 of assumed relay location R_1, then a supervisory trip signal will be sent to assist secured backup protection of HVAC grid. Similarly, the TWATs estimated using SMPA algorithm at 7 DFRs location in test system is tabulated in Table II for 48 km, 20 km, 10 km, 30 km and 50 km fault location from AC bus 2. As evident from Table II, the TW based wide area real time fault location is estimated using graph theory tool and the maximum fault location error (FLE) (14) comes out to be 0.132 % . It also correctly identifies the fault zone for Relay R_1 (Zone 1 - 40 km (80 % of L_{26}), Zone 2 - 60 km (120 % of L_{26}) and Zone 3 - 450 km(100 % of L_{26}+100 % of L_{12AC})) as observed in Table II for fault F_1.

TABLE II
PERFORMANCE OF PROPOSED WABPS FOR DIFFERENT FAULT LOCATION IN L_{23} (FAULT DISTANCE IS CALCULATED FROM BUS 2)

AFL (km)	TWAT at DFR location							Fault zone	FLE (%)
	DFR A	DFR B	DFR C	DFR D	DFR E	DFR F	DFR G		
48	0.701963	0.7004016	0.700452	0.700256	0.700104	0.700101	0.701235	Zone-3	0.068
20	0.700948	0.700166	0.700362	0.700488	0.701273	0.701270	0.701145	Zone-3	0.101
10	0.701651	0.700083	0.700278	0.700476	0.701258	0.701255	0.701063	Zone-2	0.03
30	0.701815	0.700249	0.700444	0.700404	0.701188	0.701189	0.701227	Zone-3	0.132
55	0.702020	0.700454	0.700395	0.700199	0.700983	0.700981	0.701176	Zone-3	0.051

B. Impact of fault impedance

To study the impact of fault impedance on the performance of proposed WABPS, a single phase to ground (LG) F_1 with fault impedance of 20 Ω, 60 Ω and 100 Ω is simulated at 0.7 s in L_{23} at a distance of 30 km from AC bus 2 (Node "B") in the test hybrid AC/DC system. The SMPA algorithm's performance is evaluated at DFR "B" in Fig. 6, where the estimated TWAT is 0.7002473170 s, 0.700247016 s and 0.700246932 s for 20 Ω, 60 Ω and 100 Ω respectively. It is clear from Fig. 6 that the effect of fault type has non-significant effect on proposed SMPA's algorithm accuracy for fault resistance up to 100 Ω. Concurrently, the extracted TWAT for other DFRs are estimated and tabulated in Table III and (22) & (20) of the graph theory algorithm is used to identify the fault zone and fault location.

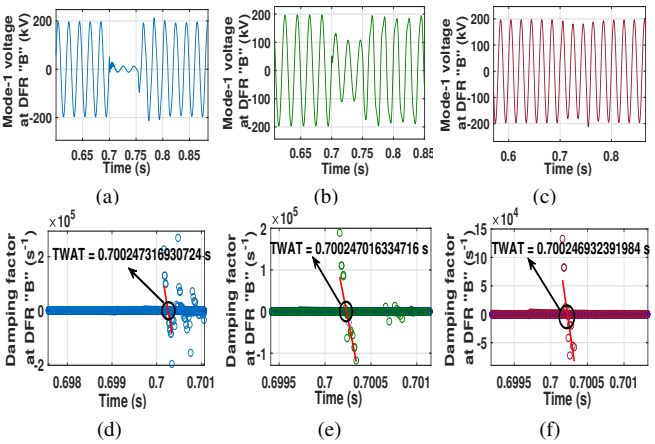

Fig. 6. Impact of fault impedance on the proposed SMPA based TWAT estimation (a) TWAT at DFR "B" for 20 Ω fault resistance, (b) TWAT at DFR "B" for 60 Ω fault resistance, (c) TWAT at DFR "B" for 100 Ω fault resistance.

C. Impact of fault type

In this subsection, the effect of fault type is initially studied on the accuracy of proposed SMPA algorithm by simulating

TABLE III
PERFORMANCE OF PROPOSED WABPS FOR DIFFERENT FAULT LOCATION & FAULT IMPEDANCE ON TRANSMISSION LINE AND CABLE IN L_{23} (FAULT DISTANCE IS CALCULATED FROM BUS 2)

Fault resistance (Ω) & AFL (km)	TWAT at DFR location							Fault zone	FLE (%)
	DFR A	DFR B	DFR C	DFR D	DFR E	DFR F	DFR G		
20 & 30	0.701813	0.700250	0.700445	0.700403	0.701188	0.701188	0.701227	Zone-3	0.125
60 & 30	0.701814	0.700251	0.700444	0.700404	0.701188	0.701188	0.701226	Zone-3	0.105
100 & 30	0.701814	0.700249	0.700444	0.700404	0.701189	0.701188	0.701227	Zone-3	0.111
20 & 80	0.702038	0.700472	0.700274	0.700079	0.700863	0.700864	0.701058	Zone-3	0.189
60 & 80	0.702036	0.700471	0.700273	0.700080	0.700865	0.700864	0.701059	Zone-3	0.192
100 & 80	0.702037	0.700472	0.700273	0.700078	0.700863	0.700864	0.701060	Zone-3	0.206

line-to-ground (LG) fault, line-to-line (LL) fault and three phase or line-line-line (LLL) fault F_1 in transmission line at 25 km distance from node B in cable between node B and D. The extracted TWAT is 0.700368071 s, 0.700360819 s and 0.700360281 s for LG, LL and LLL fault respectively as shown in Fig. 7, which indicates that the proposed TWAT estimation technique is robust against fault types. To further evaluate the performance of proposed graph theory based WABPS, the estimated TWAT at other DFRs for LG, LL and LLL fault are tabulated in Table IV. (22) and (20) are used to locate fault and identify the fault zone for relay R_1, which comes out to be zone-3. Similarly, other fault location and types are simulated in a test hybrid AC/DC grid and its performance is tabulated in Table IV, which verifies that the proposed WABPS is insensitive to different fault type.

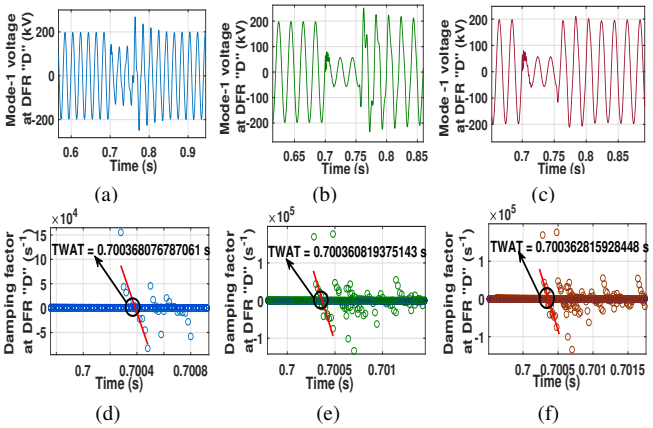

Fig. 7. Impact of fault type on the proposed fast SMPA based TWAT estimation (a) TWAT at DFR "D" for LG fault type, (b) TWAT at DFR "D" for LL fault type, (c) TWAT at DFR "D" for LLL fault type.

TABLE IV
PERFORMANCE OF WIDE AREA PROTECTION SCHEME FOR DIFFERENT FAULT LOCATION AND FAULT TYPE IN L_{23} (FAULT DISTANCE IS CALCULATED FROM BUS 2)

Fault type & distance (km)	TWAT at DFR location							Fault zone	FLE (%)
	DFR A	DFR B	DFR C	DFR D	DFR E	DFR F	DFR G		
LG & 30	0.701814	0.700252	0.700443	0.700400	0.701189	0.701187	0.701228	Zone-3	0.140
LL & 30	0.701813	0.700255	0.700441	0.700399	0.701190	0.701188	0.701230	Zone-3	0.220
LLL & 30	0.701815	0.700253	0.700440	0.700402	0.701191	0.701189	0.701231	Zone-3	0.153
LG & 55	0.702022	0.700456	0.700397	0.700201	0.700987	0.700982	0.701177	Zone-3	0.404
LL & 55	0.702021	0.700455	0.700398	0.700199	0.700984	0.700982	0.701178	Zone-3	0.521
LLL & 55	0.702020	0.700454	0.700395	0.700199	0.700983	0.700981	0.701176	Zone-3	0.382

D. Impact of LVRT control of MMC converter

There will be an impact of LVRT controller of MMC converter on the apparent impedance seen by the conventional distance (mho) relay, which is given as [21] -

$$Z_{app}^{AG} = \frac{(Res_F + pZ_L^1)I_{R_1}^a + Res_f I_{grid}^a + 3pZ_L^1 I_{tr}^0}{I_{R_1}^a + 3kI_{tr}^0} \quad (23)$$

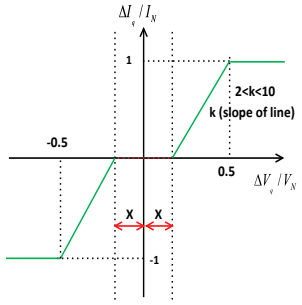

Fig. 8. LVRT control characteristics of MMC controller

Where Z^{AG}, Res_F, p, Z_L^1, $I_{Res_A}^a$, I_{grid}^a, I_{tr}^0 and k are the apparent fault (phase A to ground fault) impedance, fault resistance, per unit length, positive sequence line impedance, relay faulted phase current, grid faulted phase current, transformer zero sequence current and $k = \frac{Z_L^0 - Z_L^1}{3Z_L^1}$ respectively. In (23), the component $\frac{(Res_F + pZ_L^1)I_{R_1}^a}{I_{R_1}^a + 3kI_{tr}^0}$ highlights dependence of the apparent impedance on the converter side current (remotely contributed from bus 2), which is limited by 1.15-1.2 pu (saturation limit). The denominator part of (23) $(I_{R_1}^a + 3kI_{tr}^0)$ further dominated by positive sequence converter current (remote contribution) component, which further influence the apparent impedance trajectory seen by the relay R_1.

TABLE V
PERFORMANCE OF PROPOSED WABPS AGAINST LVRT CONTROL IN MMC CONVERTER FOR FAULT IN L_{12AC} AND L_{23}.

Fault type & AFL (km)	TWAT at DFR location							Fault zone	FLE (%)
	DFR A	DFR B	DFR C	DFR D	DFR E	DFR F	DFR G		
LG & 5 in L_{12AC}	0.201548	0.200020	0.200198	0.200390	0.201175	0.201177	0.200980	Zone-2	0.202
LL & 5 in in L_{12AC}	0.201547	0.200019	0.200200	0.200392	0.201174	0.201176	0.200981	Zone-2	0.184
LG & 20 in L_{12AC}	0.201489	0.200077	0.200274	0.200469	0.201254	0.201253	0.2010579	Zone-3	0.138
LG & 10 in L_{23}	0.201650	0.200084	0.200278	0.200475	0.201258	0.201259	0.201062	Zone-2	0.152
LL & 30 in in L_{23}	0.201812	0.200250	0.200443	0.200405	0.201188	0.201189	0.201225	Zone-3	0.140

As per the LVRT control characteristic as shown in Fig 8, the additional converter reactive current (ΔI_q) support should be directly proportional to the voltage drop (ΔV) at the PCC, expressed as $\Delta I_q = k \times \Delta V/V$, where the reactive current droop (k) can be adjusted within a range of 2-10 pu. But it does not activates if voltage drop lies within dead band of ± 0.1 pu as shown in Fig. 8.

At 0.2 s, a LG fault F_2 is simulated for 400 ms at a distance of 5 km from AC bus 2 in OHTL L_{12AC} of test hybrid AC/DC grid shown in Fig. 4, which lies in zone-2 for conventional mho relay R_1 located at bus 6 in test system. The LVRT controller of MMC converter 2 will get activated, when PCC voltage (Bus 2) falls below the threshold voltage (0.9 pu in test system) set by the grid code, during fault and it will support the converter bus (Bus 2) voltage by injecting reactive power as shown in Fig. 9(a). The grid bus (Bus 3) also contribute reactive power to the system as shown in Fig. 9(a). The active power support from MMC 2 drops down to zero during fault

as shown in Fig. 9(b). The DC current and voltage response to the AC fault F_2 is shown in Fig.9(g) and (h), which shows the recovery of HVDC grid after the fault event clearance. The apparent impedance (Z_{app}) trajectory for LG fault F_2 in the test hybrid AC/DC system, with and without HVDC, is plotted for mho relay R_1 in Fig.9(i). As evident form Fig.9(i), the mho relay correctly identifies the fault F_2 in zone-2 for test system without MMC based HVDC system, whereas the mho relay classifies the fault F_2 as zone-3 fault which highlights the underreach issue with conventional mho relay. Moreover, the SMPA based TWAT information at all DFRs are tabulated in Table V for fault F_2 with different combination of fault type and fault location in OHTL L_{12AC} and cable L_{23}.

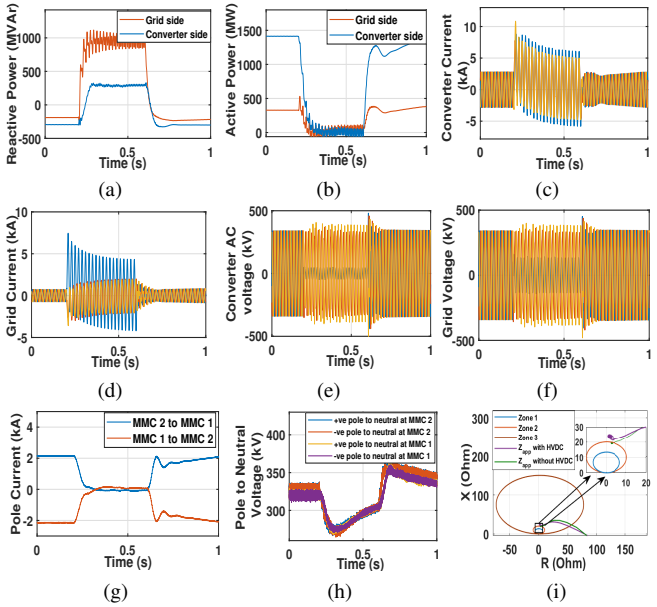

Fig. 9. Impact of LVRT control on conventional distance protection scheme (a) Reactive power flow from MMC 2 & L_{23} from bus 3, (b) Active power flow from MMC 2 & L_{23} at bus 3, (c) Current contribution from MMC 2, (d) Current contribution from L_{23} at bus 3, (e) AC voltage at MMC 2, (f) AC voltage at bus 3, (g) DC current in HVDC link, (h) DC pole voltage at MMC 1 and MMC 2 terminal, (i) Z_{app} seen by Relay R_1 with and without HVDC LVRT controller

V. Conclusion

A robust and secured TW based WABPS is designed for mixed cable & OHTL of the HVAC grid interfacing MMC converter based HVDC link. A SMPA algorithm is used to estimate TWAT in DFR located at the AC bus terminal using low sampling frequency (50 kHz) measurement and sent to WABPC via dedicated communication channel conforming to IEC-61850 communication protocol. A graph theory based wide area real time fault location is estimated and a distance protection based supervisory backup trip signal is sent to the associated circuit breaker in the HVAC grid. The performance of proposed WABPS is validated against fault types, fault resistance, fault distance, measurement noise (up to 50 dB SNR) and LVRT control of MMC converter, and its application could also be extended for wide area real time fault localization in the HVAC transmission network. While the proposed method has been validated through detailed simulations, practical implementation and field testing are key next steps. We are currently exploring collaboration opportunities with an industrial partner to evaluate the feasibility and performance of the technique in real-world conditions. This future work will focus on hardware-in-the-loop testing and measurement-based validation to further support the applicability of the proposed approach.

References

[1] M. Banafer and M. Biswal, "Investigation of power system cascading failure and the causes," in *2018 2nd International Conference on Power, Energy and Environment: Towards Smart Technology (ICEPE)*. IEEE, 2018, pp. 1–5.

[2] N. Flourentzou, V. G. Agelidis, and G. D. Demetriades, "Vsc-based hvdc power transmission systems: An overview," *IEEE Transactions on power electronics*, vol. 24, no. 3, pp. 592–602, 2009.

[3] D. Wu, G. Li, M. Javadi, A. M. Malyscheff, M. Hong, and J. N. Jiang, "Assessing impact of renewable energy integration on system strength using site-dependent short circuit ratio," *IEEE Transactions on Sustainable Energy*, vol. 9, no. 3, pp. 1072–1080, 2017.

[4] M. Sarkar, J. Jia, and G. Yang, "Distance relay performance in future converter dominated power systems," in *2017 IEEE Manchester PowerTech*. IEEE, 2017, pp. 1–6.

[5] J. Jia, G. Yang, A. H. Nielsen, and P. Rønne-Hansen, "Impact of vsc control strategies and incorporation of synchronous condensers on distance protection under unbalanced faults," *IEEE Transactions on Industrial Electronics*, vol. 66, no. 2, pp. 1108–1118, 2018.

[6] B. Kasztenny, "Line distance protection near unconventional energy sources," in *16th International Conference on Developments in Power System Protection (DPSP 2022)*, vol. 2022. IET, 2022, pp. 224–229.

[7] L. He, C.-C. Liu, A. Pitto, and D. Cirio, "Distance protection of ac grid with hvdc-connected offshore wind generators," *IEEE Transactions on Power Delivery*, vol. 29, no. 2, pp. 493–501, 2013.

[8] P. K. Nayak, A. K. Pradhan, and P. Bajpai, "Secured zone 3 protection during stressed condition," *IEEE Transactions on Power Delivery*, vol. 30, no. 1, pp. 89–96, 2014.

[9] Y. Liang, Y. Huo, and F. Zhao, "An accelerated distance protection of transmission lines emanating from mmc-hvdc stations," *IEEE Journal of Emerging and Selected Topics in Power Electronics*, vol. 9, no. 5, pp. 5558–5570, 2021.

[10] S. Paladhi and A. K. Pradhan, "Adaptive distance protection for lines connecting converter-interfaced renewable plants," *IEEE Journal of Emerging and Selected Topics in Power Electronics*, vol. 9, no. 6, pp. 7088–7098, 2020.

[11] M. Zolfaghari, R. M. Chabanlo, M. Abedi, and M. Shahidehpour, "A robust distance protection approach for bulk ac power system considering the effects of hvdc interfaced offshore wind units," *IEEE Systems Journal*, vol. 12, no. 4, pp. 3786–3795, 2017.

[12] Y. Liang, Y. Ren, and W. He, "An enhanced current differential protection for ac transmission lines connecting mmc-hvdc stations," *IEEE Systems Journal*, 2022.

[13] W. Cong, H. Zhang, H. Kong, M. Chen, and Z. Wei, "Longitudinal protection method based on voltage wave comparison in ac/dc hybrid system," *IEEE Transactions on Industry Applications*, vol. 58, no. 2, pp. 1564–1572, 2022.

[14] B. Sahoo, S. R. Samantaray, and B. R. Bhalja, "An effective zone-3 supervision of distance relay for enhancing wide area back-up protection of transmission system," *IEEE Transactions on Power Delivery*, vol. 36, no. 5, pp. 3204–3213, 2020.

[15] O. Naidu, A. K. Pradhan, and N. George, "A hybrid time-domain protection scheme for series compensated transmission lines," *IEEE Transactions on Power Delivery*, vol. 37, no. 3, pp. 1823–1833, 2021.

[16] N. Ali, B. M. Ali, M. L. Othman, and K. Abdel-Latif, "Performance of communication networks for integrity protection systems based on travelling wave with iec 61850," *International Journal of Electrical Power & Energy Systems*, vol. 95, pp. 664–675, 2018.

[17] R. J. Hamidi and H. Livani, "Traveling-wave-based fault-location algorithm for hybrid multiterminal circuits," *IEEE Transactions on Power Delivery*, vol. 32, no. 1, pp. 135–144, 2016.

[18] M. Banafer and S. R. Mohanty, "An efficient travelling wave based fault localization for mtdc transmission system," in *2021 9th IEEE International Conference on Power Systems (ICPS)*, 2021, pp. 1–6.

[19] T. K. Sarkar and O. Pereira, "Using the matrix pencil method to estimate the parameters of a sum of complex exponentials," *IEEE Antennas and propagation Magazine*, vol. 37, no. 1, pp. 48–55, 1995.

[20] S. Azizi, M. Sanaye-Pasand, M. Abedini, and A. Hasani, "A traveling-wave-based methodology for wide-area fault location in multiterminal dc systems," *IEEE Transactions on Power Delivery*, vol. 29, no. 6, pp. 2552–2560, 2014.

[21] M. M. Alam, H. Leite, J. Liang, and A. da Silva Carvalho, "Effects of vsc based hvdc system on distance protection of transmission lines," *International Journal of Electrical Power & Energy Systems*, vol. 92, pp. 245–260, 2017.